Approach to the physical origin of breakdown in silicon solar cells by optical spectroscopy

Paul Gundel,[a] Wolfram Kwapil, Martin C. Schubert, Holger Seifert, and Wilhelm Warta
Fraunhofer Institute for Solar Energy Systems (ISE), Heidenhofstr. 2, D-79110 Freiburg, Germany

(Received 31 August 2010; accepted 18 October 2010; published online 20 December 2010)

The electrical breakdown of silicon solar cells at low reverse currents has recently gained increased attention. In this study we investigate the physical properties of prebreakdown sites with high resolution spectroscopy techniques. These techniques comprise the measurement of the electroluminescence under reverse voltage, microphotoluminescence spectroscopy, and micro-Raman spectroscopy. The measurements show very high levels of stress at the prebreakdown sites, an increase in the breakdown size with applied reverse bias and redshift in the breakdown electroluminescence spectrum with increasing onset voltage. The results are tentatively explained by a lower bandgap energy at the breakdown sites, which could be caused by stress. © *2010 American Institute of Physics*. [doi:10.1063/1.3517086]

I. INTRODUCTION

When single solar cells in a module are shadowed, they are reverse-biased by the unshadowed cells in the same string depending on the module architecture. The reverse bias can reach up to −13 V, which can lead to electrical breakdown.[1] The electrical breakdown, which typically occurs in spots of 1 μm diameter or less,[2] creates excessive heat, which can destroy the module. This effect has recently drawn increased attention in the silicon solar cell research community due to the growing use of low-cost silicon (upgraded metallurgical silicon), where the occurrence of prebreakdown sites is particularly frequent.[3] These sites were categorized into three groups depending on their current-voltage (I-V) characteristics.[4] Sites, which occur at a reverse bias between 0 and −10 V, are termed "type I" breakdown. Breakdown around (−12)−14 V, which is highly correlated with recombination active defects, is labeled "type II" and breakdown above this range (−14 until −20 V) "type III." As origin of the type II sites metal precipitates could be identified,[5] type III was attributed to etch pits,[6] while contact paste remnants on the wafer surface are often believed to lead to type I breakdown.[7,8] Temperature dependent measurements, I-V measurements and carrier multiplication experiments lead to the conclusion that the physical mechanism behind type III breakdown is avalanche breakdown.[6,9] The results for type I and II are far less clear. In Refs. 4 and 10–15 breakdown sites were reported to emit light over a broad spectral range. The characteristics of these reverse electroluminescence (EL) spectra and the size of the breakdown sites in silicon solar cells have not been fully investigated yet.

In this paper, we investigated all three breakdown types by microspectroscopy techniques in order to improve the physical understanding of prebreakdown in silicon solar cells. We applied micro-Raman-spectroscopy (μ−RS) for stress[16,17] and hole density measurements[18] and microphotoluminescence spectroscopy (μ−PLS) for qualitative carrier density measurements.[19–21] For analyzing the I-V characteristics and the spectrum of the EL we used micro-Reverse bias EL (μ−ReBEL).[4] As samples, bevel polished solar cells from directly bonded wafers as model systems for clean dislocations are analyzed (schematic in Fig. 1).

II. EXPERIMENTAL

We prepared six (three of each kind) 2.5×2.5 cm^2 solar cells from polished directly bonded Czochralski (CZ) (10 Ω cm boron doped) and directly bonded floatzone wafers (FZ) (1 Ω cm boron doped). The bonding leads to a clean dislocation network at the interface between the two original wafers.[22] Before the solar cell process, the bonded wafers are bevel polished so that the dislocation network intersects the front side of the solar cell. The polishing excludes misinterpretations of the μ−ReBEL signal due to optical effects of the solar cell surface (absorption and scattering) and enables the use of μ−RS and μ−PLS, which are particularly surface sensitive. The phosphorous emitter of the cells has a sheet resistance of 75 Ω/□. The front contacts were prepared by direct evaporation of Ti/Pd/Ag and subsequent silver plating. For a low contact resistivity the cells were finally tempered at 450 °C for 25 min.

In order to get an overview over the type and location of the breakdown sites, we performed reverse bias dependent measurements (between 0 and −17 V) of the breakdown light emission with a Si CCD camera (details on the setup in

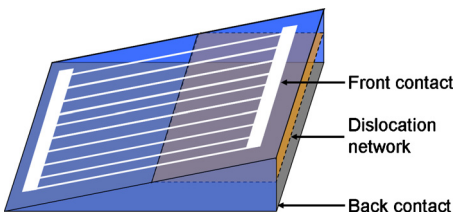

FIG. 1. (Color online) Schematic of the solar cells with bevel polished bonded wafers as starting material. The dislocation network intersects the front side in the middle of the cell.

[a]Electronic mail: paul.gundel@ise.fraunhofer.de.

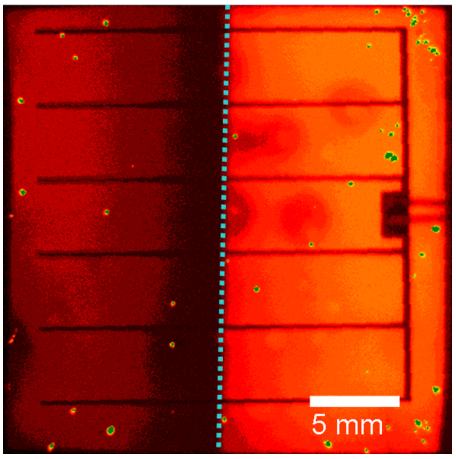

FIG. 2. (Color online) Reverse light emission (dark spots with bright surroundings) at −17 V of a FZ bonded cell. For orientation the forward EL image (bright means high forward EL emission) is shown as background. No increased breakdown occurrence is observed at the intersection between surface and dislocation network (dotted line).

Ref. 4). The 1024×1024 pixel camera yields a resolution of 25 μm on the 2.5×2.5 cm^2 cells. A sample image for the reverse light emission is shown in Fig. 2 for a FZ cell.

For the microscopic spectroscopy we used a confocal microscope, which is equipped with a Si camera for microscopic images and glass fibers, which direct the emitted light to either a 600 G mm^{-1} grating and a Si line camera for the spectroscopic analysis between 400 nm and 1000 nm wavelength or a 150 G mm^{-1} and an InGaAs line camera for the infrared region between 900 and 1500 nm wavelength. For μ−RS the 600 G mm^{-1} can be replaced by an 1800 G mm^{-1} grating. As lenses a numerical aperture (NA) 0.65 50× for μ−ReBEL and μ−PL is used, for μ−RS and the high-resolution μ−ReBEL (HR-ReBEL) a NA 0.9 100× is utilized. The spatial resolution of the spectrally resolved μ−ReBEL/HR-ReBEL measurements is 10 μm/0.4 μm. For gathering the reverse bias spectra it is crucial to correct the microscope system including all optical components for its relative quantum efficiency. This was done by calibrating the microscope with both detectors using a calibration lamp with a known spectrum. The combination of the InGaAs and the Si detector enable spectroscopic measurements between 0.8 and 3.2 eV. Details on the microscope setup are discussed in Refs. 18–21.

III. RESULTS

In order to identify sites of prebreakdown, the voltage dependent overview images are evaluated for each breakdown site and the camera counts are plotted against the reverse bias (Fig. 3).

Most of the breakdown light emission sets on around −4 to −6 V. The light intensity is very high. Both facts point toward early breakdown (type I). These plots reveal only one type II breakdown site in the FZ cell and the CZ cell and support the result of Ref. 5, that metallic impurities but not clean dislocations or oxygen, which is present in the CZ sample, cause type II breakdown. Forward reversed EL images reveal, that the breakdown sites are not correlated with recombination active areas for the type I breakdowns. Furthermore only one type III breakdown is visible. The absence of type III sites can be attributed to the polishing of the front surface, which avoids etch pits. The light intensity-voltage curves show, that the light emission of the type I and II breakdown sites is approximately linear and slightly saturates for voltages above −14 V. The saturation is probably caused by the carrier flux limitation due to series resistance between contact and breakdown site.[15]

After this localization of breakdown sites, several sites are investigated in more detail. First we measured the spectrum of the sites with μ−ReBEL at −17 V. The spectra are shown in Fig. 4 for different voltages of onset and are similar to the spectra reported in Refs. 14 and 23 for avalanche breakdown and expand these reports by virtue of the InGaAs detector down to 0.8 eV. All spectra show a distinct peak between 1.6 and 2.3 eV. The existence of a maximum in the observed range is supported by the increasing intensity with energy below 1 eV measured by the InGaAs detector, which is particularly sensitive (external quantum efficiency >70%) in this energy range. However in Ref. 15 no maxi-

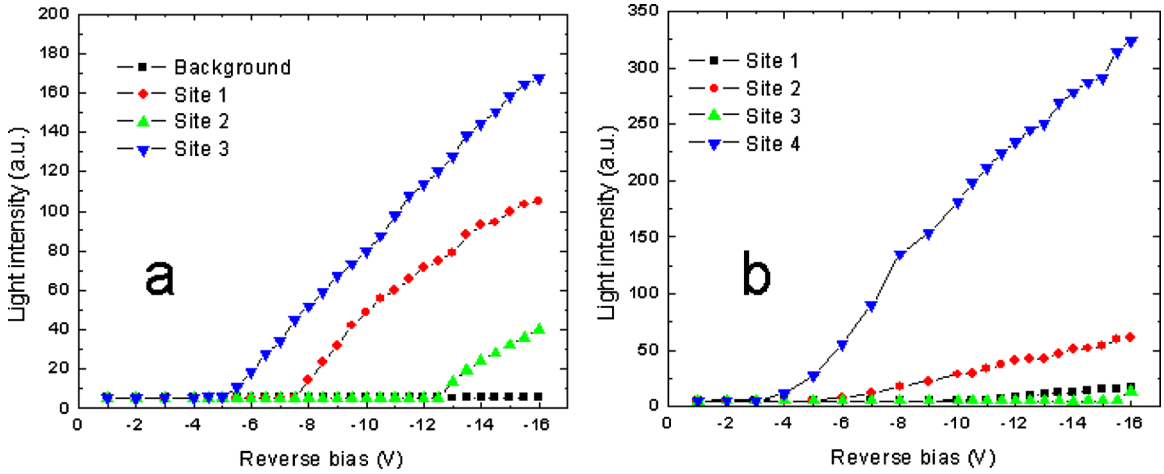

FIG. 3. (Color online) Light intensity against reverse bias for different prebreakdown sites for the FZ solar cell (a) and the CZ solar cell (b). For comparison in (a) the background on a spot on the cell without prebreakdown is shown, for (b) the background is the same. Many more (about 30) prebreakdown sites show the same characteristic as sites 1 and 3 in (a) and sites 4 and 2 in (b), for a better readability only these sites are shown.

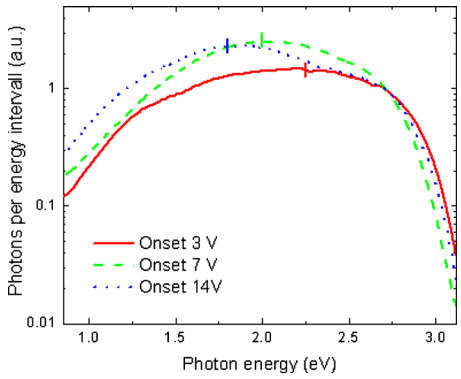

FIG. 4. (Color online) Spectra of three different prebreakdown sites with onset voltages of 3 V (type I), 7 V (type I), and 14 V (type II). The spectra are normalized to the intensity at 2.7 eV. The maxima of the spectra are marked by a vertical line. The spectra are normalized to their values at 2.7 eV to allow a comparison of the high energy characteristics.

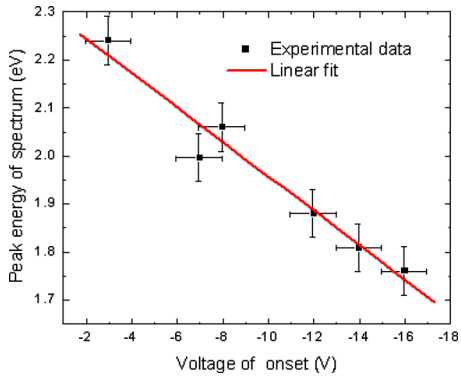

FIG. 6. (Color online) Peak position of the reverse EL spectra against the voltage of onset for six sites of prebreakdown. The errors are mainly caused by the difficulty to exactly determine the point of onset from the measurements and the flatness of the spectra. A linear decrease in the peak energy with increasing onset voltage is evident.

mum was reported, which could be due to the stated low sensitivity of the used detector for low energies.

The applied voltage has no significant effect on the shape of the spectrum (Fig. 5), which is in agreement with Ref. 15 but the position of the peak shifts linearly to lower energies with increasing onset voltage of the specific breakdown site (Fig. 6). This effect is independent of the type of breakdown.

In order to clarify whether the breakdown light emission is homogeneous in space, we scanned a breakdown site [site 1 in Fig. 3(a)],onset voltage 12 V, type II) with HR-ReBEL in the spectral range between 1.6 and 1.96 eV (around the peak of the spectrum at 1.85 eV) at −17 V applied voltage. In Fig. 7(a) the integrated intensity between 1.9 and 1.96 eV is depicted and shows a clear round spot. This image is very similar to the integrated intensity between 1.6 and 1.96 eV [Fig. 7(b)]. The spectral center of mass [Fig. 7(c)] demonstrates that the spectrum is shifted toward lower energies with increasing distance from the center. This effect could be explained by absorption of higher energy photons in the silicon. Figure 7(d) shows the integrated intensity between 1.6 and 1.65 eV, which has a "donut" halo structure. This halo structure excludes the absorption effect as single origin of the photon energy shift and shows, that electrons spread away from the center and lose parts of their energy by interaction with other electrons and the silicon lattice. Therefore, low energy photons are primarily emitted around the actual breakdown site, whereas high energy photons are emitted in the center.

Next the size of this breakdown site is investigated in dependence of the applied reverse voltage by means of the optical microscope and the 100× lens, which yield a resolution of 0.4 μm. In Ref. 13, an increase in the diameter of the breakdown site with increasing voltage was predicted due to a spreading of the charge carriers. We verify this effect and show that the diameter of this breakdown site is about 0.5 μm [Fig. 8(a)].

Since the size of the breakdown site is close to the spatial resolution of the microscope, the experimental data is somewhat scattered but still clearly shows the increase in the diameter of the site.

At the same breakdown site, we conducted μ−PLS and μ−RS measurements without applied voltage. The measure-

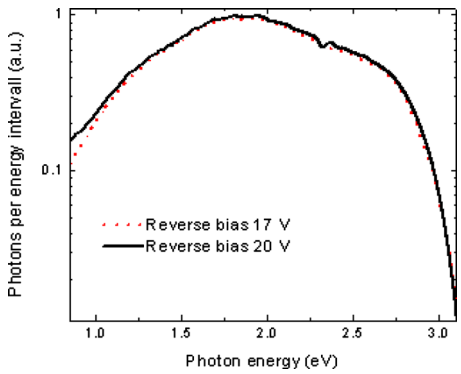

FIG. 5. (Color online) Spectra of a prebreakdown (onset voltage 16 V, type III) site at 17 V and 20 V. The spectra are practically indistinguishable above 1 eV. The higher intensities below 1 eV for 20 V could be caused by a higher number of low energy photons, which spread from the breakdown site (compare Fig. 6).

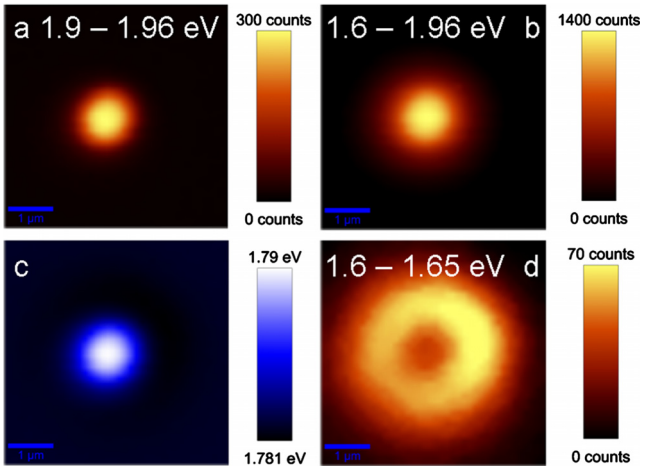

FIG. 7. (Color online) Intensity map with HR-ReBEL between 1.9 and 1.96 eV photon energy (a), intensity between 1.6 and 1.96 eV (b), which shows that the most photons originate from the center of the breakdown site and the influence of photons from outside the center on the spectrum is comparatively low. (c) shows the spectral center of mass of the spectral range between 1.6 and 1.96 eV, which lays between 1.78 and 1.79 eV and (d) the intensity between 1.6 and 1.65 eV. All images show the exactly same region.

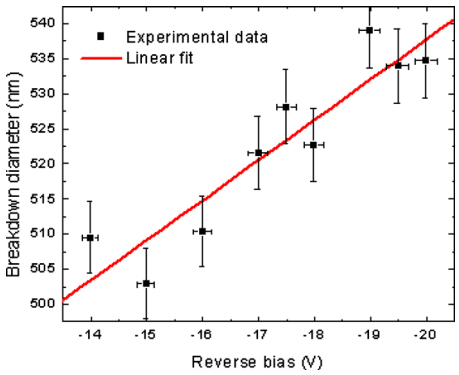

FIG. 8. (Color online) Diameter of the prebreakdown site 2 from Fig. 3(a) (type II) against reverse bias. The size was extracted from microscope images and fitting a Gaussian to a line scan across the breakdown site. The error of the diameter is caused by the fact that 500 nm is close to the spatial resolution of the microscope (400 nm) and the error in the Gaussian fit of the line scan. Still the increase in the diameter with reverse bias is significant.

ments show that high stress is present at the breakdown site [Fig. 9(b)], and a blurry brighter spot in the μ−PLS image [Fig. 9(a)], which could be due to an inhomogeneity in the recombination activity or the doping concentration. However, Fano measurements at high injection levels [Fig. 9(c)] (Ref. 18) at the site reveal an increased carrier lifetime at the breakdown site. At low excitation levels no inhomogeneity in the doping concentration[24] is apparent. The reason for the measured increased carrier lifetime is unclear and could be caused by optical effects at surface scratches. However, in microscope images no surface damages are visible. At all breakdown sites, which are correlated with contact paste remnants we measured extremely high tensile stress levels, which are sufficiently strong to lift the degeneracy of the three usually degenerated first phonon modes [Fig. 9(d)].

IV. DISCUSSION AND CONCLUSION

Since the spectra of all breakdown types are very similar to avalanche breakdown spectra in the literature[13,14] and in Ref. 25 tunneling breakdown is demonstrated to emit no photons, we conclude that avalanche breakdown is mainly responsible for the reverse EL at all breakdown sites independently of their type. Measured spectra at tunneling breakdown in Ref. 13 may be caused by the fact, that both mechanisms occur often in an intermixed state.[12] This means, that avalanche plays a significant role in all breakdown sites of silicon solar cells, while tunneling breakdown might additionally occur at some sites.

The spectra of the reverse EL show a linearly decreasing peak position with increasing on-set voltage independent of the applied reverse voltage. This gives insight in the mechanism of prebreakdown in silicon solar cells. The observed effect means that either the carriers have a higher mean energy at the breakdown sites that set on at a lower reverse voltage or the breakdown of these sites occurs closer to the surface and less high energy photons are absorbed in silicon. This absorption effect, however, is not visible in the spectral range at energies above 2.7 eV, where the absorption effect should be particularly strong due to the high absorption coefficient of silicon. In Refs. 14, 25, and 26 the origin of the breakdown luminescence is discussed and bremsstrahlung of

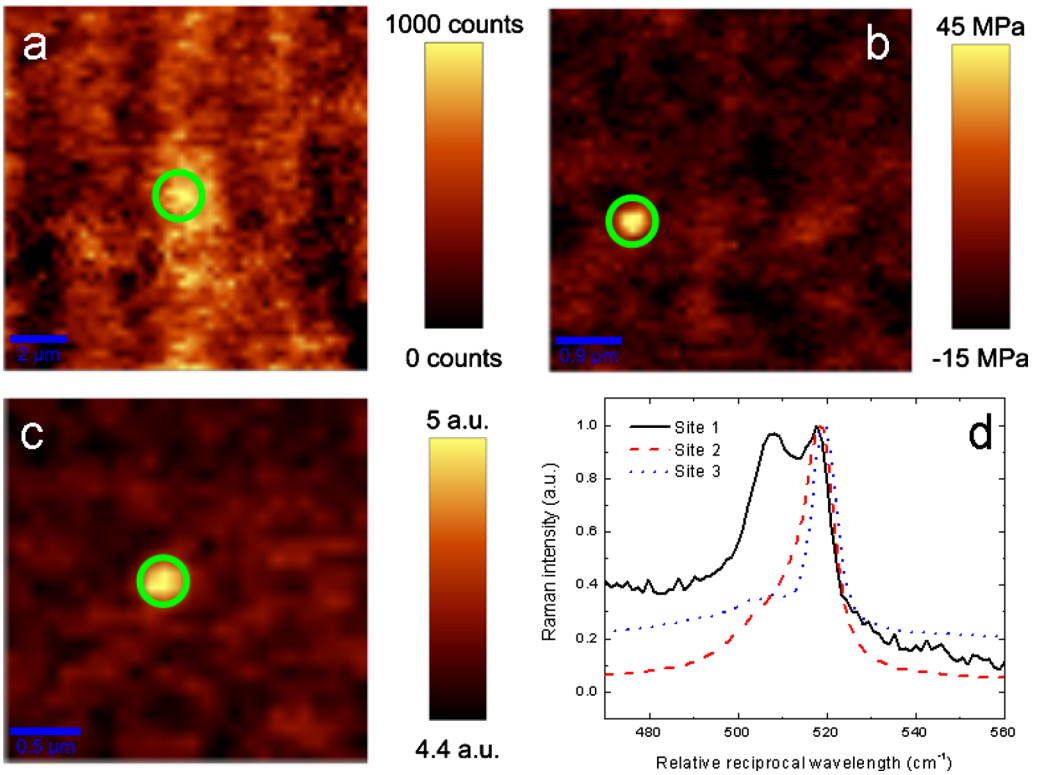

FIG. 9. (Color online) μ−PLS intensity (integrated between 1 and 1.15 μm wavelength) map (a), μ−RS stress map (b), Fano measured hole density at high injection (c) at the breakdown site from Fig. 7 in arbitrary units (type II). The position of the breakdown site is marked by the circle. (d) Shows Raman spectra of the first order silicon peak at three representative type I breakdown sites with lifted degeneracies of the first order peak.

intraband and interband transitions are mentioned as likely sources of the breakdown luminescence. Our results imply that the sooner breakdown occurs, the higher is the energy of these transitions. This is in accordance with a decreased bandgap energy E_G at the breakdown site since the energy of the intraband transitions E_{IB} is $E_{IB}=E_i-E_G$,[14] with the initial carrier energy E_i. A lower bandgap energy at the breakdown sites could also explain the low breakdown voltage, since the breakdown voltage is about proportional to the bandgap.[27] One parameter that can decrease the bandgap energy is stress.[28]

In Ref. 29, stress was demonstrated to reduce the breakdown voltage and the effect was linked to the stress induced bandgap reduction, which decreases the onset of avalanche breakdown.[29] Our μ−RS measurements show extremely high levels of tensile stress at the breakdown sites, which can change the bandgap energy significantly.[28,30] This is an indication that the stress induced bandgap reduction might be indeed involved in lowering the breakdown voltage. However, also other mechanisms such as inhomogeneities in the doping concentration, high potentials at precipitates[31,32] or etch pits[6] and other stress related effects as piezoresistance[33] might contribute to this effect. Also the causes for the high stress fields (precipitates and crystal defects) might induce the breakdown via other mechanisms. The reason for the measured higher carrier lifetime and its effect on the breakdown characteristic are not yet clear.

Additionally our spectroscopic measurements show, that electrons spread away from the breakdown site and lose parts of their energy [Fig. 7(d)] by electron–lattice and electron–electron interaction. The interaction of the electron with the lattice leads to heating of the solar cell and possibly to the destruction of the module. The remaining energy of the spread electrons is not sufficient to cause avalanche breakdown. But when the applied voltage is increased, these electrons gain sufficient energy to increase the size of breakdown site (Fig. 8), while the electron energy in the center of the breakdown site and the mean electron energy do not increase with applied voltage (Fig. 5).

Our sophisticated cell structure with the clean dislocations intersecting the depletion region shows, that clean dislocations are not an origin of prebreakdown.

In conclusion we showed the spectral and spatial distribution of the breakdown emission, the influence of applied voltage and onset voltage on these distributions, and demonstrated that clean dislocations do not increase the breakdown site occurrence and that prebreakdown sites are correlated with high stress fields. These results are in accordance with a lowering of the bandgap and consequently the breakdown voltage by stress.

ACKNOWLEDGMENTS

We gratefully acknowledge measurements by Christian Majenz and sample preparation by Nicole Bayer, Mira Kwiatkowska, Harald Lautenschlager, Gisela Räuber, and Manfred Reiche (Max-Planck-Institute for Microstructure Physics). This work was supported by internal funding of the Fraunhofer Society.

[1] M. C. Alonso-García, J. M. Ruíz, and F. Chenlo, Sol. Energy Mater. Sol. Cells **90**, 329 (2006).
[2] R. H. Haitz, A. Goetzberger, R. M. Scarlett, and W. Shockley, J. Appl. Phys. **34**, 1581 (1963).
[3] V. Hoffmann, K. Petter, J. Djordjevic-Reiss, E. Enebakk, J. T. Håkedal, R. Tronstad, T. Vlasenko, I. Buchovskaja, S. Beringov, and M. Bauer, Proceedings of the 23rd European Photovoltaic Solar Energy Conference, Valencia, Spain, September 2008, pp. 1117–1120.
[4] W. Kwapil, M. Kasemann, P. Gundel, M. C. Schubert, W. Warta, P. Bronsveld, and G. Coletti, J. Appl. Phys. **106**, 063530 (2009).
[5] W. Kwapil, P. Gundel, M. C. Schubert, F. D. Heinz, W. Warta, E. R. Weber, and A. Goetzberger, Appl. Phys. Lett. **95**, 232113 (2009).
[6] J. Bauer, J.-M. Wagner, A. Lotnyk, H. Blumtritt, B. Lim, J. Schmidt, and O. Breitenstein, Phys. Status Solidi (RRL) **3**, 40 (2009).
[7] J. W. Bishop, Sol. Cells **26**, 335 (1989).
[8] D. Lausch, K. Petter, R. Bakowskie, C. Czekalla, J. Lenzner, H. von Wenckstern, and M. Grundmann, Appl. Phys. Lett. **97**, 073506 (2010).
[9] O. Breitenstein, J. Bauer, J.-M. Wagner, and A. Lotnyk, Prog. Photovoltaics **16**, 679 (2008).
[10] A. G. Chynoweth and K. G. McKay, Phys. Rev. **102**, 369 (1956).
[11] W. Mönch, Phys. Status Solidi **36**, 9 (1969).
[12] A. G. Chynoweth and K. G. McKay, J. Appl. Phys. **30**, 1811 (1959).
[13] G. Deboy and J. Kölzer, Semicond. Sci. Technol. **9**, 1017 (1994).
[14] N. Akil, S. E. Sterns, D. V. Kerns, Jr., A. Hoffmann, and J.-P. Charles, Appl. Phys. Lett. **73**, 871 (1998).
[15] M. Schneemann, A. Helbig, T. Kirchartz, R. Carius, and U. Rau, Phys. Status Solidi A **207**, 2597 (2010).
[16] I. De Wolf, Semicond. Sci. Technol. **11**, 139 (1996).
[17] M. Becker, H. Scheel, S. Christiansen, and H. P. Strunk, J. Appl. Phys. **101**, 063531 (2007).
[18] P. Gundel, M. C. Schubert, F. D. Heinz, J. Benick, I. Zizak, and W. Warta, Phys. Status Solidi (RRL) **4**, 160 (2010).
[19] P. Gundel, M. C. Schubert, W. Kwapil, J. Schön, M. Reiche, H. Savin, M. Yli-Koski, J. A. Sans, G. Martinez-Criado, W. Seifert, W. Warta, and E. R. Weber, Phys. Status Solidi (RRL) **3**, 160 (2009).
[20] P. Gundel, M. C. Schubert, and W. Warta, Phys. Status Solidi A **207**, 436 (2010).
[21] P. Gundel, F. D. Heinz, M. C. Schubert, J. A. Giesecke, and W. Warta, J. Appl. Phys. **108**, 033705 (2010).
[22] M. Reiche, Mater. Sci. Forum **590**, 57 (2008).
[23] M. Lahbabi, A. Ahaitouf, M. Fliyou, E. Abarkan, J.-P. Charles, A. Bath, A. Hoffmann, S. E. Kerns, and D. V. Kerns, Jr., J. Appl. Phys. **95**, 1822 (2004).
[24] M. Becker, U. Gösele, A. Hofmann, and S. Christiansen, J. Appl. Phys. **106**, 074515 (2009).
[25] M. du Plessis and P. Rademeyer, Solid-State Electron. **54**(4), 433 (2010).
[26] P. A. Wolff, Phys. Chem. Solids **16**, 184 (1960).
[27] S. M. Sze and G. Gibbons, Solid-State Electron. **9**, 831 (1966).
[28] W. Paul and D. M. Warschauer, J. Phys. Chem. Solids **5**, 89 (1958).
[29] A. Goetzberger and R. H. Finch, J. Appl. Phys. **35**, 1851 (1964).
[30] I. Balslev, Phys. Rev. **143**, 636 (1966).
[31] R. Lal and R. Sharan, Solid-State Electron. **29**, 1015 (1986).
[32] W. Kwapil, M. Wagner, M. C. Schubert, and W. Warta, J. Appl. Phys. **108**, 023708 (2010).
[33] C. S. Smith, Phys. Rev. **94**, 42 (1954).